AD-A081 659 CALSPAN ADVANCED TECHNOLOGY CENTER BUFFALO NY F/G 20/4
EXPERIMENTAL INVESTIGATION OF SIMULITUDE PARAMETERS GOVERNING T--ETC(U)
1980 C PADOVA, T J FALK, C E WITTLIFF F44620-76-C-0057

UNCLASSIFIED NL

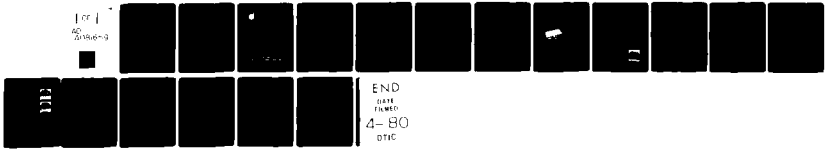

END
DATE FILMED
4-80
DTIC

Unclassified

SECURITY CLASSIFICATION OF THIS PAGE (When Data Entered)

REPORT DOCUMENTATION PAGE

READ INSTRUCTIONS BEFORE COMPLETING FORM

1. REPORT NUMBER: AIAA-80-0158
2. GOVT ACCESSION NO.:
3. RECIPIENT'S CATALOG NUMBER:

4. TITLE (and Subtitle): Experimental Investigation of Similitude Parameters Governing Transonic Shock-Boundary Layer Interactions

5. TYPE OF REPORT & PERIOD COVERED: AIAA Paper

6. PERFORMING ORG. REPORT NUMBER:

7. AUTHOR(s): C. Padova, T. J. Falk, and C. E. Wittliff

8. CONTRACT OR GRANT NUMBER(s): F44620-76-C-0057 ~~N00014-76-C-0630~~ N00019-77-C-0179

9. PERFORMING ORGANIZATION NAME AND ADDRESS: Calspan ~~Corporation~~, Advanced Technology Center, P. O. Box 400, Buffalo, New York 14225

10. PROGRAM ELEMENT, PROJECT, TASK AREA & WORK UNIT NUMBERS: Task No. 061-185

11. CONTROLLING OFFICE NAME AND ADDRESS: Office of Naval Research, Department of the Navy, 800 N. Quincy Street, Arlington, Virginia 22217

12. REPORT DATE: January 1980

13. NUMBER OF PAGES:

14. MONITORING AGENCY NAME & ADDRESS (if different from Controlling Office):

15. SECURITY CLASS. (of this report): Unclassified

15a. DECLASSIFICATION/DOWNGRADING SCHEDULE:

16. DISTRIBUTION STATEMENT (of this Report):

17. DISTRIBUTION STATEMENT (of the abstract entered in Block 20, if different from Report):

DTIC ELECTE FEB 25 1980 S D A

18. SUPPLEMENTARY NOTES:

19. KEY WORDS (Continue on reverse side if necessary and identify by block number)

Reynolds Number
Boundary Layer
Turbulent
Transonic
Normal Shock Wave
Shock-Induced Boundary-Layer Separation
Heat Transfer
Pressure Gradient

20. ABSTRACT (Continue on reverse side if necessary and identify by block number)

For a 2D transonic shock-boundary layer interaction, the effects of wall-to-total temperature ratio and of flow constraints imposed downstream of the shock have been investigated experimentally. A normal shock wave was established in a M = 1.43 flow over a flat plate in a Ludwieg tube at a flow length Reynolds number varying from 9 x 10^6 to 36 x 10^6. Stream total temperature was varied in the range 265°K to 350°K, and the effects on shock configuration and flow variables were measured. The skin friction and velocity profiles were found to be affected, but the pressure distribution and shock

DD FORM 1 JAN 73 1473 EDITION OF 1 NOV 65 IS OBSOLETE

Unclassified

SECURITY CLASSIFICATION OF THIS PAGE (When Data Entered)

configuration remained nearly unchanged. A summary plot of these and earlier results shows that the separated length depends only weakly on Re_{δ_u} but that it increases strongly with Mach number and stream temperature. In order to explore the effect of a diverging flow field downstream of the shock, such as that which might be encountered on an airfoil, a shock holder having a perforated top wall was tested. The shock bifurcation height and the length of the separated region were both found to increase strongly with the degree of the downstream flow divergence.

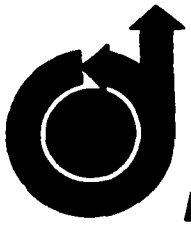

AIAA-80-0158

Experimental Investigation of Similitude Parameters Governing Transonic Shock-Boundary Layer Interactions

C. Padova, T. J. Falk and
C. E. Wittliff, Calspan Advanced
Technology Center, Buffalo, N.Y.

$2.00

A 21

AIAA 18th AEROSPACE SCIENCES MEETING

January 14-16, 1980/Pasadena, California

41

(6)

EXPERIMENTAL INVESTIGATION OF SIMILITUDE PARAMETERS GOVERNING TRANSONIC SHOCK-BOUNDARY LAYER INTERACTIONS*

(10) C. Padova** T.J. Falk* C.E. Wittliff*
Calspan Advanced Technology Center
Buffalo, N.Y.

(12) 17
(11) 1980

Abstract

For a 2D transonic shock-boundary layer interaction, the effects of wall-to-total temperature ratio and of flow constraints imposed downstream of the shock have been investigated experimentally. A normal shock wave was established in a M = 1.43 flow over a flat plate in a Ludwieg tube at a flow length Reynolds number varying from 9 x 10^6 to 36 x 10^6. Stream total temperature was varied in the range 265°K to 350°K, and the effects on shock configuration and flow variables were measured. The skin friction and velocity profiles were found to be affected, but the pressure distribution and shock configuration remained nearly unchanged. A summary plot of these and earlier results shows that the separated length depends only weakly on Re_{δ_u} but that it increases strongly with Mach number and stream temperature. In order to explore the effect of a diverging flow field downstream of the shock, such as that which might be encountered on an airfoil, a shock holder having a perforated top wall was tested. The shock bifurcation height and the length of the separated region were both found to increase strongly with the degree of the downstream flow divergence.

Nomenclature

A	Cross-sectional area
C_f	Skin friction coefficient (referenced to sonic conditions)
H	Boundary layer profile shape factor, δ^*/θ
h	Open height of shock holder exit
L	Length of flat plate
l	Generic flow length
l_s	Length of separated flow region
M	Mach number
p	Pressure
Re_L, Re_{δ_u}	Reynolds number based on plate length and undisturbed boundary layer thickness, respectively
T	Temperature
t	Time
u	Streamwise velocity
W	Mass flow rate per unit area
X	Streamwise coordinate, in model frame of reference
x	Streamwise distance from shock wave
y	Normal coordinate
α	Streamline angle
δ	Boundary layer thickness
δ^*	Displacement thickness
θ	Momentum thickness or Heat transfer parameter
λ	Height of bifurcated shock wave
σ	Ratio of open-to-closed area in perforated shock holder

Subscripts and Superscripts

K	At location of kink in surface pressure distribution
o	At stagnation
R	At start of surface pressure rise
S	At location of the onset of flow separation (does not apply to l_s)
u	In the undisturbed flow ahead of interaction
w	At the wall
δ	At the edge of boundary layer
λ	At bifurcation point
*	Critical flow conditions (M = 1); does not apply to δ^*

Introduction

Scaling of transonic wind tunnel data to full scale conditions when a shock wave-turbulent boundary layer interaction is imbedded in the flow remains one of the important unsolved problems in aerodynamic applications. In the late sixties, the conventional technique of simulating Mach number in the overall flow and compensating for full scale Reynolds number (Re_L) effects on the viscous layer by producing artificially early transition were found to have serious shortcomings[1, 2]. More than a decade of effort in the development of new testing facilities and in the experimental investigation of the interaction phenomena has followed. The latter has produced a fairly consistent phenomenological description of the interaction over a range of some of the governing parameters. However, unresolved features are still present and no set of criteria which permit modeling at less than full scale Re_L has emerged. Recently the development of cryogenic wind tunnels for high Reynolds testing has added new emphasis to problems related to temperature effects.

The results of a Calspan investigation of the effects of Reynolds number changes (at high Reynolds numbers) on the transonic (M ≈ 1.4) shock-wave boundary-layer interaction on a flat plate have been reported earlier[3]. This paper is con-

*Sponsored by AFOSR, Contract No. F44620-76-C-0057, by ONR, Contract No. N00014-76-C-0630 and by NAVAIR, Contract No. N00019-77-C-0179.

**Research Engineer.

*Principal Engineer.

cerned with the results of two sets of experiments designed to explore the effects of changes in two additional similarity parameters: the ratio of wall-to-total temperature and the geometry of the subsonic flow boundary downstream of the interaction. The experiments may serve any of several purposes by providing a description of the phenomena which result from changes in the parameters considered, by supplying a local picture of the flow field which may be patched into a larger description of the flow field in the vicinity of an airfoil, or by supplying data which may be used to anchor the theoretical codes which are now becoming capable of attacking the same interaction problem.

The flow region that is of concern in studies of separated transonic shock-wave boundary layer interactions is sketched in Fig. 1. Three basic experiments may be used to simulate this flow region. First, an airfoil may be used to generate a supercritical flow and shock embedded in an essentially subsonic stream. Alternatively a bump on a wind tunnel wall may accomplish the same objective. Finally a shock generator (holder) may be used to develop the desired shock structure in a fully supersonic incoming stream. The experiment reported here belongs to the last category, the choice having been made on the basis of using a large scale model to permit a detailed probing of the interaction and to provide a high test Re_L. Thus, only a neighborhood of the wave/viscous interaction occurring on an airfoil is simulated. In Fig. 1 this is characterized by multiples (n,m) of a characteristic interaction length (l) to be specified. Natural choices for the latter length could be: any distinctive length of the viscous layer (δ, for example), the length, of the characteristic shock bifurcation in the inviscid field (λ) or the length of the region of separated flow (l_s), when this occurs.

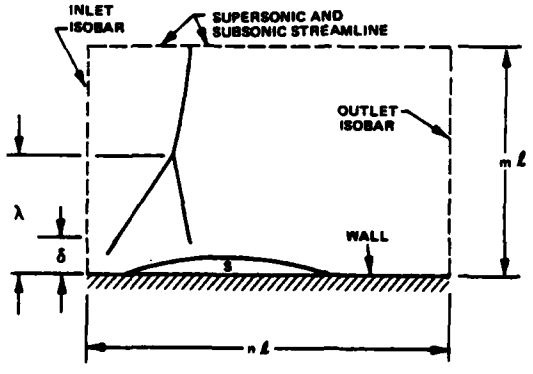

Fig. 1 Typical region for local shock-boundary layer interaction simulation.

The first series of experiments reported here may be viewed as an attempt to simulate under varying heat transfer conditions the shock wave-boundary layer interaction standing on a flat plate in an unconfined flow. To the extent that the dimensions of the interaction region are small compared with those of an airfoil the experiment can also be considered to represent a first approximation to a local description of the shock-boundary layer interaction occurring on an airfoil. This approximation may not always be a good one as we shall see later. In the second series of experiments the boundary conditions downstream of the shock were changed in a manner which would impose an adverse pressure gardient on an unseparated flow. This is a situation which may arise on the surface of an airfoil when the interaction region is long enough so that the effect of the non-parallel airfoil flow field becomes significant within the interaction length.

For the experimental results to be of maximum use, conditions at the boundaries of the observed interaction neighborhood should be completely determined. In the case of the ideal flat plate this is, at least in principle, easily accomplished. The incoming flow would be described by a viscous surface boundary layer together with the uniform parallel inviscid flow field only slightly modified by the presence of the boundary layer on the plate. The upper boundary surface, provided that it can be located far enough from the plate, consists of a streamline parallel to the plate. It is isobaric and supersonic upstream of the shock and isobaric and subsonic downstream of the shock. Provided that the outlet surface is located far enough downstream, it also is isobaric and contains a fully developed viscous layer consistent with the local inviscid flow. The outlet flow field, however, is more complicated than the inlet flow since the bifurcated shock introduces a slip surface. The flow length required for this slip surface to disappear completely might, depending upon the height of the bifurcation, be very long and in a reasonable experiment it is more probable that the slip surface will be smoothed but not eliminated completely.

In neither of the two experiments reported here was the flow at the boundaries as simple as described above. In these experiments, as well as in most other experiments of similar type, the top boundary was too close to satisfy completely the requirements for unconfined flow. This results from a compromise between the need to obtain a high test Reynolds number and the intolerance of the transonic flow field to the blockage effect associated with the increase in boundary layer displacement thickness through the shock wave. Although the effect is believed not to be large, the top wall of the shock holder imposes a flow inclination which is not necessarily that which would exist at the same height in an unconfined flow. In the second series of experiments the flow inclination at the top plate was deliberately chosen to be different from the unconfined flow. The flow angle near the top plate was then measured to complete the data set.

Experiment Description

Wind Tunnel Facility

The Calspan Ludwieg tube[4] is a large scale, upstream diaphragm facility as shown in the schematic of Figure 2A. The supply tube is 18.3 m long and has an inner diameter of 1.1 m. At the downstream end there is located a diaphragm station which houses a quick release cutter bar. The transonic cylindrical nozzle, which follows, is housed within a large dump tank 2.4 m in diameter and 18.3 m long. The nozzle consists of an entrance section with area contraction of 1.72:1, followed by a constant area section 0.813 m in diameter and 2.44 m long. The constant area of the nozzle is perforated to a porosity of 19.1%.

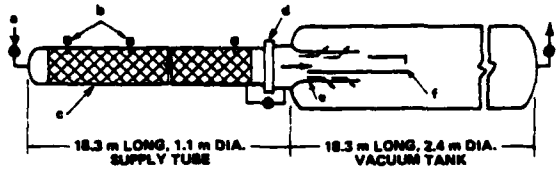

A. TEST APPARATUS IN LUDWIEG TUBE

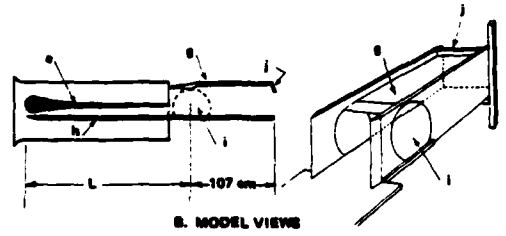

B. MODEL VIEWS

(a) DRY, COMPRESSED AIR SUPPLY; (b) FIVE, EVENLY SPACED THERMOCOUPLES; (c) WRAP-AROUND HEATERS; (d) DIAPHRAGM AND CUTTER; (e) NOZZLE WITH TAYLORED POROSITY DISTRIBUTION; (f) 33 x 40 cm MODEL; (g) SHOCK HOLDER TOP PLATE; (h) FLAT PLATE (L = 124 cm OR 241 cm); (i) OBSERVATION WINDOW; (j) CHOKING FLAP

Fig. 2 Test apparatus.

The perforated nozzle is contained within the evacuated dump tank, and during the experiment sonic outflow through the walls expands the nozzle flow to low supersonic Mach numbers. Selective coverage of some of the perforations permits streamwise variation of the Mach number. In the present experiment this feature was used to reproduce an airfoil-type pressure history in the boundary layer approaching the shock. Figure 2B shows one of 17 elements of the perforation pattern which are equally spaced around the nozzle. A detailed description of the nozzle design and pressure distribution is given in Ref. 3.

In the operation of the Ludwieg tube, a Mylar diaphragm is inserted at the diaphragm station, the nozzle and dump tank are evacuated to a predetermined pressure, the supply tube is pressurized, and the diaphragm is ruptured mechanically. After the transient starting process is completed, a steady flow is obtained until an expansion wave travels up the supply tube, reflects from the end wall, and returns to the nozzle. Originally, the test time of the facility was about 45 ms. Later the facility was lengthened, and all the experiments discussed here were performed with about 95 ms of useful test time available.

The early operation of the Ludwieg tube was limited to experiments with the entire apparatus initially equilibrated to room temperature. At those conditions, the expansion wave propagating into the supply tube accelerated the gas and cooled it to a total temperature of about 265°K. This produced a wall-to-total temperature ratio of about 1.11 and resulted in heat transfer from the model to the gas. In order to obtain heat transfer from the gas to the model, the total temperature was increased by heating the entire supply tube with electrical heaters mounted around the exterior surface. This modification allowed the supply tube to be heated to as high as 550°K. In the present experiments, temperatures up to about 400°K were utilized. With the hot supply tube, the test gas heated up during the pressurization process and equilibrated at a uniform temperature very quickly. Five thermocouples mounted within the supply tube were used to measure the initial gas temperature and to verify its uniformity.

Model Description and Operation

The flow channel and shock holder used in this experiment were designed with the objective of simulating the flow through a normal shock wave standing on an airfoil at nearly full scale Reynolds number. In all experiments an airfoil-type pressure history was imposed upon the boundary layer approaching the shock. In two separate series of experiments the boundary conditions downstream of the shock were treated differently, however. First the interaction was allowed to develop in a flow channel which was of approximately constant cross-sectional area except for an area increase in the immediate vicinity of the shock. In an inviscid one-dimensional flow this area increase, which was required to stabilize the shock position, would have imposed an adverse pressure gradient upon the subsonic flow immediately downstream of the shock. In fact it can be seen in some of the schlieren pictures that the flow separates from the top wall and the effect of the area change may have been negated. Later the shock holder was changed to provide better control of the streamline shape at the top wall. The second experimental series described in this paper was formulated in response to the observation that on an airfoil the length of the interaction region is often large enough so that significant changes in pressure can be expected to occur over its length. The new shock holder permitted changes to be made in the boundary condition downstream of the shock so that the effect of an adverse pressure gradient downstream of the shock could be investigated.

The flat plate shock holder assembly is shown schematically in Fig. 2B. The flat boundary layer plate spanned the 81 cm width of the nozzle and extended either 124 cm or 241 cm upstream of the shock position. An additional 107 cm of plate constituted the bottom wall of the shock holder flow channel. A steady boundary layer flow, as evidenced by pitot pressure, static pressure and skin friction is established on the floor plate about 15 ms after the start of the experiment. This is consistent with the time required to establish turbulent boundary layers as measured in Ref. 5.

The flow downstream of the nozzle exit is constrained by a rectangular shock holder flow channel 40.6 cm wide with height depending, as described later, on the geometry used for the upper shock holder plate. The side walls of the rectangular channel extend a few centimeters into the nozzle exit and divert the thick nozzle boundary layer. The flow is choked with an adjustable flap at the exit of the shock holder channel. It is this flap that, during the starting process, sends a shock wave system upstream through the channel and produces the desired shock wave-boundary layer interaction.

The selection of the shock holder which is used to stop the traveling shock wave and stabilize it at a fixed position is an important aspect of the experimental design. A propagating shock can be weakened and positioned at a fixed location by

decreasing the mass flow per unit area behind it. This can be accomplished by introducing an area change in the flow channel or by removing mass along the shock holder. In the two sets of experiments discussed in this paper both schemes were used. The shock holder flow channel used in the temperature ratio investigation is the early one described in Ref. 3. It is recalled schematically in Fig. 3A. The channel entrance height is 28 cm. The area change is formed by a ramp on the top wall of the shock holder, 10 cm long, which increases the flow channel height to 33 cm. During the starting process the choking flap sends a wave system upstream through the channel. The upstream progress of the wave system is halted by the area change. The normal shock wave so formed remains stable at its test position for a period of 6 to 15 ms, which is adequate to permit the flow to stabilize and the data to be taken.

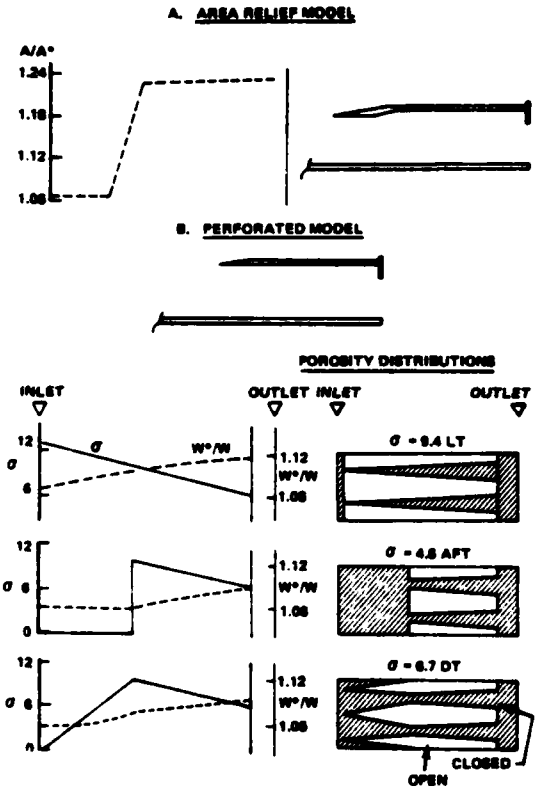

Fig. 3 Model configurations.

The later tests used mass removal through the top wall to stabilize the shock. The ramp was removed from the top wall and replaced by perforations (12.5% open area) that extend from 2.8 cm behind the leading edge to a point near the exit of the model. Removal of the ramp increased the entrance height to 33 cm, and the resultant channel is one of constant cross-sectional area. With this shock holder the wave system can be stabilized nearly anywhere along the length of the model either within the model or external to its forward lip. In general stationary shock structures lasting 15 to 25 ms are found to be possible with this model.

By blocking some of the perforations in the top plate it was possible with this configuration to vary the boundary conditions downstream of the shock wave. Three different perforation distributions are compared with the original area relief shock holder in Fig. 3. A simple one-dimensional (1D) characterization of the flow is used to describe each shock holder. The area relief holder is described in terms of the variation along its length of the ratio of local cross-sectional area to the critical value for the flow downstream of a normal shock at the test Mach number (A/A*). Idealized reference values for all flow quantities are then available using 1D, isentropic relationships. The perforated shock holder is described in terms of the variation along its length of the ratio of the critical mass flow per unit area (for the flow downstream of a normal shock at the test Mach number) to the local mass flow per unit area (W*/W). In calculating the latter, the outflow through the perforations was taken to be that which would occur if the choked outflow were driven by the full stagnation pressure downstream of a normal shock with an orifice coefficient equal to 1.0. In the 1D characterization, the quantity W*/W corresponds directly to the quantity A/A* of a constant-mass-flow-rate channel and comparison of any flow quantity occurring in the porous or area relief holder configuration is straightforward.

The three different porosity distributions of Fig. 3B are labeled according to their average open area as percentage of the total top wall area (σ). The streamwise distribution of σ along the top wall is also given in each case. In the first (top to bottom) configuration σ varied linearly from the leading edge of the plate, where the full 12.5% of porosity of the top plate was open, to a point near the choking flap, where half the perforations were closed off. The average porosity was therefore 9.4% and the configuration is designated 9.4 Linearly Tapered. In the second configuration, called 4.6 AFT, the open area was concentrated toward the downstream (aft) end of the plate and the average porosity was 4.6%. In the third configuration the average porosity was 6.7% and the open area was doubly tapered. Tests were also made using other configurations but only the above three are discussed in this paper. Prior to the tests the possibility existed that changing the shock holder to the perforated configuration and the resulting change in the downstream boundary condition might increase the length of the separated flow region but not influence greatly the flow in the immediate neighborhood of the shock foot. In fact, as will be seen later, large changes in the shock structure were observed.

Instrumentation

The basic instrumentation and data reduction procedure used in this apparatus are described in Ref. 3. In summary, the instrumentation includes a set of pitot-static rakes, any of which may be mounted on a 12.7 cm long base plate containing the pressure transducers. The base plate may be mounted flush with the floor plate at various stations along the flow channel. In addition, a second plate shown in Figure 4 incorporates a set of 10 pressure orifices and transducers and 10 piezoelectric skin friction transducers. This plate may also be located at various streamwise positions to generate closely

spaced pressure and skin friction data points. In various tests, pressure transducers have also been mounted at fixed positions along the floor plate to measure the pressure distribution along the full length of the model.

All of the transducers used in the basic instrumentation are piezoelectric devices developed at Calspan. They are described in Ref. 6 and 7. Each transducer is compensated internally to minimize acceleration effects and, typically, they are linear to within ±2%. The pressure transducers have a full-scale range of 690 kPa and a nominal sensitivity of 7.25 mv/kPa. The skin friction transducers have a 6.4 mm diameter sensing surface and can measure skin friction up to 140 Pa. Typically, they have a skin friction sensitivity of 3ט20 mv/kPa and a pressure sensitivity of 0.7 to 3.0 mv/kPa. The skin friction transducers were calibrated for pressure sensitivity and corrections were applied to the skin friction data. This was accomplished using the surface pressure measured adjacent to each skin friction transducer, Fig. 4.

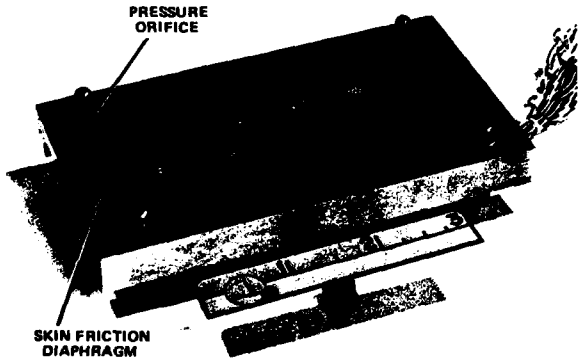

Fig. 4 Skin friction survey plate.

Schlieren observations of the flow field were made using a high speed framing camera operating at a rate of about 7000 frames per second. This diagnostic was used to determine the shock position along with other structural features of the flow monitored.

Recently, in order to complete the data, a flow angle probe has been added to the instrumentation deployed during the tests. This probe, oriented to measure pitch angle, is used to record the flow angle at a plane 4.0 cm below the top wall. The flow angle probe, which consists of two tubes mounted side by side and beveled at ±45°, was calibrated in a separate continuous flow tunnel at M = 0.6 and 0.9. Its calibration was found to be the same for these two Mach numbers and the same calibration was assumed to hold in all of the flow angle probe data reduction.

Discussion of Data and Preliminary Analysis

Undisturbed Velocity Profiles

In the present study a wall-wake model[8] is adopted to represent the mean flow quantities of the undisturbed boundary layer. As pointed out early by Seddon[9] and confirmed subsequently by others, this choice is appropriate. In the incoming flow, a logarithmic law of the wall representation provides a well documented link with the skin friction at the wall. Downstream of the interaction, the tendency of the boundary layer to return to an equilibrium profile represented by the universal law of the wall is also well-established. However, through the interaction, the law of the wall representation is not satisfactory and, therefore, a description of the flow field in terms of the more fundamental integral parameters is desirable.

Fitting the measured velocity profile to the wall-wake model allows calculation of the conditions defining the flow at the inlet of the interaction. They are presented in Table I for the two sets of test conditions discussed in this paper. The exponent n for a power law model of the velocity profiles, $y \sim u^n$, is also retained in the table because of its value of quick reference and adequacy in flows with zero pressure gradient.

A degree of arbitrariness is contained in Table I. In compressible flow the reduction procedure from rake pressure measurements to velocity profiles is an approximate one. This results in a dependence of the reduced velocity profile on physical assumptions made and empirical constants required (for example, recovery factor). When deriving characteristic or integral parameters from the velocity profiles, the error intrinsic to the approximation is susceptible to amplification or reduction, depending on the calculation procedure. The latter, in turn, is constrained by the amount of instrumentation deployed in the test, namely skin friction balances, temperature probes, etc. Only limited concurrence is found in the literature on the relative accuracy of commonly used data reduction procedures in relation to flow regimes and principal parameters of interest[10,11,12]. This available basis, however, confirms the judgment that the uncertainty associated with the values of Table I is irrelevant in relation to the quantitative understanding of the shock wave-boundary layer interaction set forth in this and previous studies.

Table I

UNDISTURBED VELOCITY PROFILE PARAMETERS

SET	Re_L	M	T_w/T_o	δ (mm)	δ^* (mm)	σ (mm)	H	n	$C_f \times 10^3$
I	36×10^6	1.43	0.85	17.0	3.26	1.68	1.94	7.1	1.6
	36×10^6	1.46	1.0	21.1	3.79	1.67	2.26	7.8	1.5
	36×10^6	1.46	1.11	23.9	4.08	1.67	2.44	8.1	1.4
II	36×10^6	1.43	1.11	34.0	5.96	2.64	2.26	8.1	2.3
	9×10^6	1.43	1.11	34.6	6.62	2.73	2.42	7.4	2.5

Test sets I and II differ both with respect to the test flow conditions and the model. For the temperature ratio investigation (set I), the boundary layer was allowed to develop on a 1.2 m long plate. Adjustments in the supply tube charge pressures were used to control the density of the test flow so that a constant Re_L of 36×10^6 was obtained with any of the selected test flow temperatures. For the subsonic boundary condition investigation (set II), the boundary layer devel-

oped on a 2.4 m long plate. The constant temperature ratio of 1.11 corresponded to Ludwieg tube operation at room temperature. Operation at charge pressures of 35 and 138 kPa resulted in the test Re_L of 9 x 10^6 and 36 x 10^6, respectively. A representative sample of the measured boundary layers entering the interaction for both plate lengths and constant Reynolds number are shown in Fig. 5.

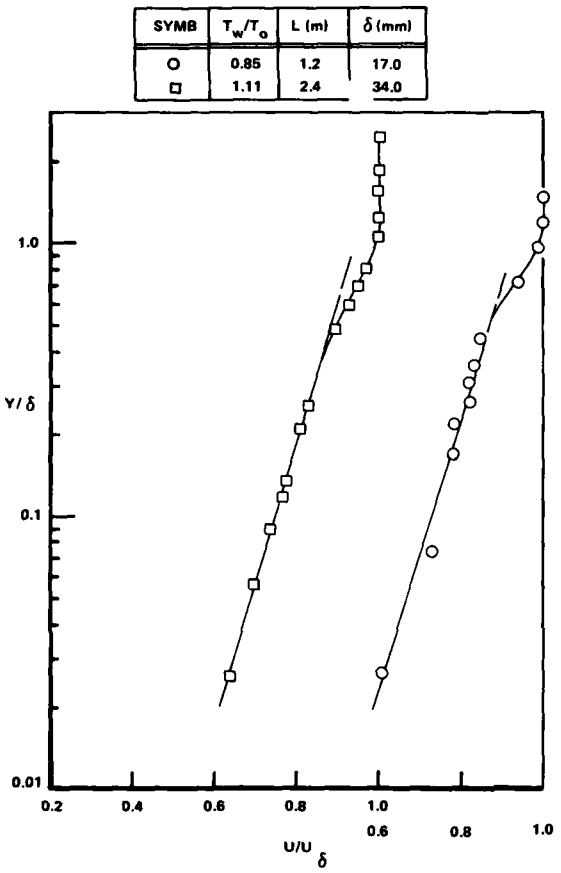

Fig. 5 Undisturbed velocity profiles, Re_L = 36 x 10^6, M = 1.43.

Boundary layer calculations using the integral method computer program of Ref. 13 were performed to provide a quantitative framework in which to estimate the effects of test condition variables as well as transition uncertainty on the present experiment. Calculations at the free temperature ratios of interest and free stream conditions matching the experimental ones confirm[14] the measured trends of δ^* increasing, form factor H increasing, and skin friction decreasing as the wall goes from slightly cool to slightly hot. It is found that differences between the computed and measured values of the above parameters diminish if the natural transitional regime between instability and full turbulence computed by the program is reduced. The Schlichting-Ulrich-Granville method is used to predict natural transition in the program. In the experiment, early transition of the boundary layer close to the plate leading edge is anticipated based on model geometry and the noise generated in the test flow by the perforated nozzle. By adopting the option, available in the program, of forcing transition early along the plate, it was possible to obtain quite satisfactory agreement between experiment and computation with respect to C_f. Agreement was less satisfactory with respect to boundary layer thickness.

This residual disagreement between predicted and measured values of the undisturbed boundary layer entering the interaction does not affect the measurements of concern in this experiment. For the present purpose, the direct measurements are to be used and their accuracy is satisfactory. However, the disagreement evidenced is relevant and, indeed, could be very important when scaling of flows containing shock boundary layer interactions is attempted. It also substantiates the judgment that the derivation of similarity criteria for a flow region confined to the neighborhood of the interaction constitutes a simpler and prerequisite step to more rigorous scaling procedures for practical airfoil flows.

Wall-To-Total Temperature Ratio Effect on the Interaction

Heating the Ludwieg tube air supply while keeping the model at room temperature produced interactions at T_w/T_o = 0.85, 1.0, 1.11. The 1.2 m long boundary layer plate and the area relief shock holder were used. Nominal test conditions were Re_L = 36 x 10^6 and M = 1.43 or 1.46. Under these conditions T_w/T_o = 0.97 corresponds to adiabatic flow. Thus the extreme temperature ratios tested represent symmetrical cases of heat transfer from the flow to the wall and vice versa.

The effect of varying T_w/T_o on the development of the boundary layer prior to entering the interaction was discussed in the preceding paragraph. For the shock wave-boundary layer interaction, the measurements of relevant scales, surface pressures and skin friction distributions with varying temperature ratio are described in the following.

Height of bifurcation - The height of the shock pattern is recorded in the schlieren movies. A frame that is typical of the flow configuration under steady conditions is presented in Fig. 6.

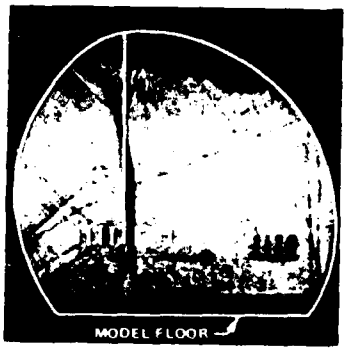

Fig. 6 Observed shock structure, area relief model, T_w/T_o = 0.85.

The normal shock is positioned at the ramp of the area relief shock holder (the ramp is located above the center of the nine tick marks on the

observation window). The oblique waves in the field-of-view are located within the dump tank but external to the test section. They were eliminated in subsequent tests by fairing a small discontinuity in the flow plate existing at the model-nozzle junction outside of the test section side wall. The flow on the upper wall at the shock holder shows a large displacement. Extensive separation appears to have occurred. On the model flat plate, the growth of the boundary layer through the interaction region is evidenced by the darker region of flow close to the bottom of the field-of-view in the schlieren picture.

The height of the bifurcation point has been scaled from pictures similar to the one presented. This height, 5.6 cm, is found to be nearly constant with variation in the temperature parameter. The slight variations in bifurcation height that were observed are of order ±8mm, an amount comparable with the uncertainty in the height measurement. There is some indication of a trend for the bifurcation height to increase as T_w/T_o becomes larger. Nevertheless, when the bifurcation height is normalized by the undisturbed boundary layer thickness, λ / δ_u, the measurements indicate an essentially constant, normalized height λ / δ_u = 2.75 for the present tests at M = 1.46 and Re_L = 36 x 10^6. This corresponds to stating that the changes in the vertical extent of the interaction as a result of varying T_w/T_o are totally due to changes occurring in the incoming boundary layer.

The invariance of λ / δ_u with temperature ratio is quite revealing when considered together with the measured effect of T_w/T_o on the longitudinal extent of the interaction. In the following it is shown that decreasing T_w/T_o increases the length of the region of separated flow. At a fixed Mach number, the height λ / δ_u is governed by how far the first disturbance in the incoming boundary layer propagates upstream of the normal shock and by how fast the thickness of the layer increases immediately downstream of the first disturbance. If a region of separated flow is present, the above viscous quantities are expected to be related to the extent of the separation. This can coarsely be described by the length and the height of the separation bubble. The observed behaviour of λ / δ_u, then, rules out changes in the height of the separated flow region as T_w/T_o is varied. This is certainly so at the foot of the bifurcation and most likely even downstream. These circumstances imply a degree of uncoupling between two phases of the viscous layer development through the interaction. The separation phase, occurring at the bifurcated foot, is dominated by inertia and pressure forces and is unaffected by temperature changes. The momentum equalization phase occurring downstream of the bifurcated foot, is sensitive to density gradients and is found to be very dependent on the T_w/T_o parameter.

Wall pressure distributions - In the temperature effect investigation, surface pressures were measured piecewise along the center line of the model. Streamwise distributions were obtained by joining pressure measurements taken over the length of the pressure plate described previously, that is, over 10 cm segments. Fixed test conditions were maintained for the tests required to cover the desired streamwise range. The relative distance to the normal shock was derived from the correlation of the schlieren record and the pressure traces at fixed time. Overlapping of sequential pressure segments and run repetition provided the desired consistency check.

The pressure distributions show the general pattern that is well established for all transonic shock wave-turbulent boundary layer interactions that have been studied experimentally. The location of the start of the interaction occurs approximately two undisturbed boundary layer thicknesses upstream of the bifurcation point. An initial linear sharp pressure rise to a kink pressure (as termed in airfoil work by Pearcey and others) occurs and is followed by a slower nonlinear pressure rise tending asymptotically downstream toward the value expected for a normal shock. The ratio of kink pressure to upstream pressure is unaffected by the temperature parameter and has a value of about 1.55.

The relationship between kink pressure and separation pressure is an important element in the description of the interaction. The degree of correlation between the location of the kink pressures, and the location of the separation point, defined by the criterion C_f = 0 (see following Fig. 9 and 10) is shown in Fig.7. It is seen

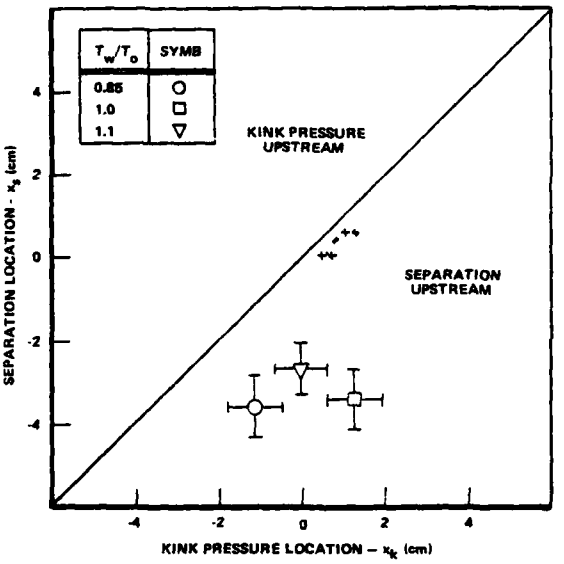

Fig. 7 Correlation of kink pressure and separation points.

that the present data do not support the conclusion that the kink pressure corresponds to the occurrence of separation in the flow. Separation, as indicated by C_f = 0, appears here to occur slightly upstream of the kink pressure. No consistent trend with T_w/T_o can be detected within the accuracy of the data. After the kink location the pressure variation remains smooth. No definite indication of the occurrence of reattachment can be detected, pointing to some degree of decoupling between the pressure field and the velocity field when this region of the interaction has been reached. Thus, nothing can be inferred with respect to the influence of the temperature on reattachment from the surface pressure distribution alone. In contrast, the percentage of the normal shock recovery that is reached far downstream of the

interaction at a fixed distance is found to be clearly affected by the temperature parameter. For example, at 30 cm from the pressure rise 88.1% pressure recovery of the normal shock value was obtained for T_w/T_o = 0.85, decreasing to 85.1% for T_w/T_o = 1.0 and 82.1% for T_w/T_o = 1.11.

Since the three sets of pressure data discussed here differ in the value of the undisturbed boundary layer entering the interaction, it is relevant to determine whether accounting for such a scaling factor alone explains the measured temperature effect on the surface pressure distribution. This is indeed the case as confirmed by Fig. 8. Here, the pressure measurements are

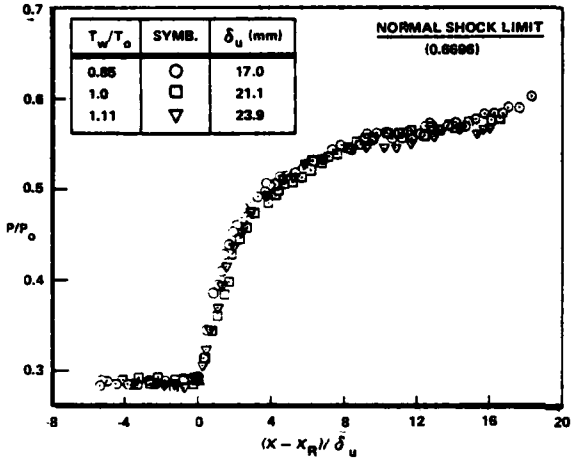

Fig. 8 Heat transfer effect on wall pressure distribution, Re_L = 36 x 10^6, M = 1.46.

shown plotted as a function of distance from the start of the pressure rise ($X-X_R$) normalized by the undisturbed boundary layer thickness δ_u. Within the scatter of the data, it is not possible to discern a variation with the T_w/T_o. As pointed out earlier, minor changes in the nozzle porosity that occurred during test phases resulted in measurements at a freestream Mach number slightly different ($\Delta M = 0.03$) for T_w/T_o = 0.85 and T_w/T_o = 1.0 and 1.11. This difference has been accounted for in Fig. 8. As a result of the consistent comparison at fixed M and Re_L, it can be stated that the T_w/T_o variation in the range of the present experiment shows no influence on the surface pressure distribution through the interaction. In particular, this is true for the percentage of normal shock pressure recovery far downstream of the interaction which has a value of 86 (±1.5)% at 16 undisturbed boundary layer thicknesses downstream of the first pressure rise.

Skin friction distributions - Tangential stresses acting on the flat plate surface were measured throughout the interaction region with the skin-friction tranducers. Fig. 9 and 10 present the distribution of the skin friction coefficient, C_f, as a function of streamwise distance from the location of the bifurcation point, for the two extreme values of T_w/T_o. The values of C_f result directly from normalization of the measured tangential stresses by a reference dynamic pressure chosen, for the present data, at sonic flow condition. Each C_f distribution, like the wall

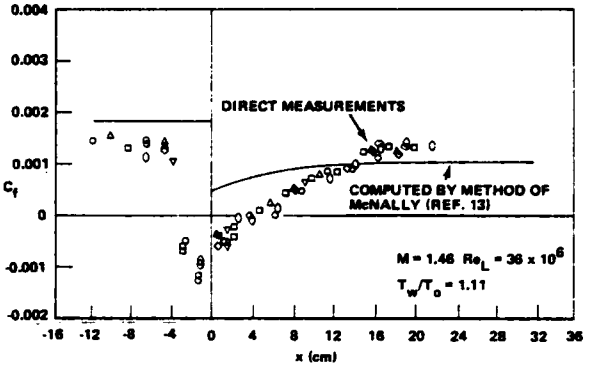

Fig. 9 Skin friction distribution, T_w/T_o = 1.11.

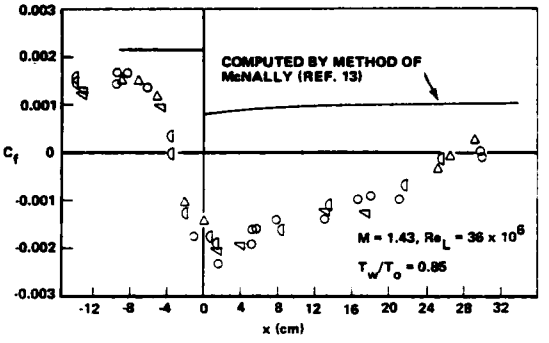

Fig. 10 Skin friction distribution, T_w/T_o = 0.85.

pressure distributions, was obtained by joining piecewise measurements.

The measured effect of varying the temperature ratio on the skin friction distribution may be seen by comparing Fig. 9 and 10. The length of the separated flow region is found to be very sensitive to variations in the T_w/T_o parameter. It should be noted that the measurements were taken along the center plane of the flow channel and any possible variation of separation and reattachment points across the width of the channel is neglected. In the figures, the length of the separated region corresponds with the region of negative C_f. As the temperature ratio decreases from 1.11 to 0.85, l_s increases from 6.3 to 30.5 cm. Insight to the mechanisms affecting the separated flow region is offered by details of the skin friction distributions. The onset of separation relative to the location of the normal shock wave remains nearly unchanged as T_w/T_o decreases, as does the sharp drop down to the negative minimum. In contrast, the slope of the linear rise toward positive values decreases remarkably with T_w/T_o. As a result, reattachment of the flow occurs farther downstream of the normal shock location when T_w/T_o has a lower value. It is thus the momentum transfer in the predominantly subsonic flow region downstream of the shock that is affected by the thermal gradient characteristic of the incoming boundary layer.

The data for T_w/T_o = 1.0 and 1.11 show a fairly well defined positive plateau downstream of reattachment. The C_f level reached is respectively, 47% and 96% of the undisturbed value. In the data for T_w/T_o = 0.85, the separated flow

region extends more than 25 cm downstream of the normal shock location, and the available skin friction measurements do not extend beyond the region of linear C_f rise. An indication of the adjustments in skin friction that are to be expected, due only to the imbalance of momentum and mass flow rate that occurs in the sudden transition from supersonic to subsonic flow, was sought by simple boundary layer computations. The same momentum and moment-of-momentum integral equations that were used to compute the growth of the undisturbed boundary layer were solved with initial conditions specified by the displacement and momentum thicknesses at the start of the interaction and subsonic outer flow. The subsonic inviscid flow conditions used were the ideal ones valid downstream of a M = 1.46 normal shock, that is, M = 0.716 and total pressure 94.3% of p_o. The computations show a monotonic decrease of the shape parameter, H, toward an equilibrium value nearly independent of the temperature ratio. The decrease in H is accompanied by a marked reduction in δ^* before the equilibrium growth rate is established. This reduction in δ^* is strongly temperature ratio dependent. As a consequence of these velocity profile adjustments, the skin friction behaves as the solid line plotted in Figs. 9 and 10. A sudden temperature independent reduction by a factor of about 1.35 in C_f is computed to satisfy the equations with the given initial conditions. From this level a rise, dependent on temperature ratio, is computed up to a maximum beyond which the equilibrium decrease takes over (not shown in the figures).

The interesting features that are common to measurements and computations are: a) the rates of C_f rise to equilibrium downstream the shock show the same trend with changes in the temperature parameter, b) the values of the C_f plateaus that precede equilibrium growth display similar increases in terms of percentages of the undisturbed values as T_w/T_o is increased. While simple boundary layer computations such as the ones presented are well known to be inadequate to predict shock-boundary layer interactions, in light of the above they offer some relevant indications.

The experimentally observed temperature effect on the length of the separated region, appears to result from the combination of two mechanisms. The pressure-jump-induced viscous-inviscid interaction, which dominates the onset and early separation region, causes a negative jump in C_f. The magnitude of this jump decreases as T_w/T_o increases. The velocity equilibration in the boundary layer, which is predominant during the progression toward reattachment, causes the C_f value to approach its plateau value more rapidly when T_w/T_o increases. In combination these effects cause reattachment to occur more quickly when T_w/T_o is high. This interpretation is better illustrated by Fig. 11. The differences in the values of the undisturbed boundary layer entering the interaction that exist for the three temperature ratios tested have been accounted for by replotting each skin friction distribution with streamwise distance normalized by δ_u. The origin of the abscissa is taken at the point of separation x_s. In combination with Fig. 8 describing wall pressures, Fig. 11 well illustrates the magnitude of the temperature ratio effect on the length of the separated flow and the

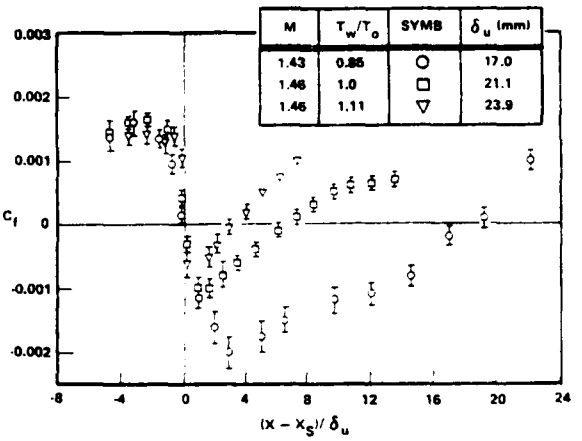

Fig. 11 Heat transfer effect on skin friction distribution, $Re_L = 36 \times 10^6$.

post-shock, momentum-transfer-related character of this effect.

Velocity profiles through the interaction - Pitot and static pressure surveys were made in the interaction zone. These surveys were used to infer velocity profiles. Ideally, a very fine mapping of the velocity field throughout the interaction is desirable, because it is the velocity vector changes that display the details of the viscous-inviscid coupling dominating the phenomena. Both streamwise and transverse (normal to the flat plate) components of the velocity vector are relevant, since the flow deviates remarkably from its initial boundary layer character. Direct detection of flow angularity is, in fact, anticipated to be a capability pacing the advancement of the understanding of shock boundary layer interactions. However, only longitudinal velocity components were measured in the T_w/T_o investigation. Practical limitations to the desired detailed mapping of the longitudinal component velocity field were also encountered.

Velocity profiles obtained at a temperature ratio of 0.85 and Reynolds number of 36 x 10^6 are presented in Fig. 12. The local velocity u has

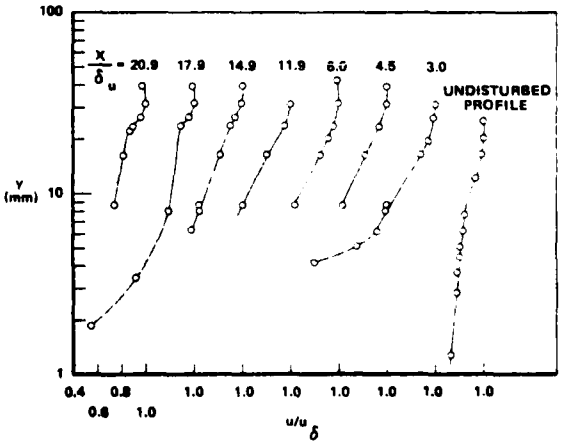

Fig. 12 Velocity profiles, $Re_L = 36 \times 10^6$, M = 1.43, $T_w/T_o = 0.85$.

been normalized by the velocity u_δ at the edge of the viscous layer and is presented in semi-logarithmic plot versus the distance y normal to the wall. Individual profiles are labeled with the distance, in the model reference frame, of the station at which they were taken. Such distance, X, has been normalized by the value of the undisturbed boundary layer thickness δ_u. Semilogarithmic plots of the boundary layer velocity profiles readily indicate the deviations of the boundary layer from its equilibrium form described by the wall-wake model, as the interaction is traversed. First, the logarithmic region that is well-defined between y = 0.5 mm and y = 7.6 mm in the undisturbed boundary layer, is found to decrease in extent and in slope. This occurs when the boundary layer is retarded due to the pressure rise in the interaction region. Separation has occurred upstream of $X/\delta_u = 3.0$ and the area of reversed flow which is characteristic of this region, is indicated by the height at which $u/u_\delta = 0$ is obtained. These findings are in good agreement with the skin friction data. Throughout the separation region, the slope of the residual logarithmic portion of the velocity profiles remains fairly unchanged. At a distance $X/\delta_u \approx 12$ the velocity profiles evolve rapidly in slope in the logarithmic region. However, mutations in the inner portion of the boundary layer appear to trail somewhat behind. Skin friction distribution data indicate reattachment taking place at $X/\delta_u \approx 16$. The boundary layer growth, indicated by the two independent direct measurements is thus consistent. Overall, the velocity profile measurements substantiate the observations of the previous section on the mechanisms at play in shaping the temperature effect on the interaction phenomena.

Subsonic Boundary Effect on the Interaction

Seven porosity distributions covering, values 12.5, 9.4, 6.7, 4.6, 2.2, and 0% average porosity, were used to change the subsonic boundary condition downstream of the interaction. Mass removal was variously concentrated toward the front or the rear of the holder. Porosity selection is determined by the desired pressure gradient but is constrained by the requirements for obtaining a stable shock in the appropriate position within the flow time available in the Ludwieg tube. The test time required for shock wave formation at the choking flap and its trajectory toward the holder lip depend significantly on p_o, the ratio of p_o to vacuum tank pressure, the porosity magnitude and distribution, and the choke flap setting. Only a coarse range of choke settings was used with each porosity in the initial test which was performed to explore subsonic boundary effects and to investigate the apparatus limits. As a result only some of the porosity/choke setting combinations gave rise to stable shock patterns. Three such combinations having stable bifurcations within the field of view of the schlieren at both Re_L = 36 x 10^6 and 9 x 10^6 have been singled out for discussion. Measurements for the solid case ($\sigma = 0$), which gave a stable shock only at the lower Re_L are also presented.

Bifurcation height and location - With all of the porous holder configurations tested, a well defined shock structure was observed to move into the field of view at a speed between 10 and 20 ms^{-1} depending on the test parameters. A nearly normal upper wave branch and a tall bifurcated foot form the structure. Typically the height of the bifurcation is observed to undergo minor changes as the upper normal shock travels within the model, Fig. 13A (and position "a" in the sketch of Fig. 14). The schlieren photographs in Fig. 13

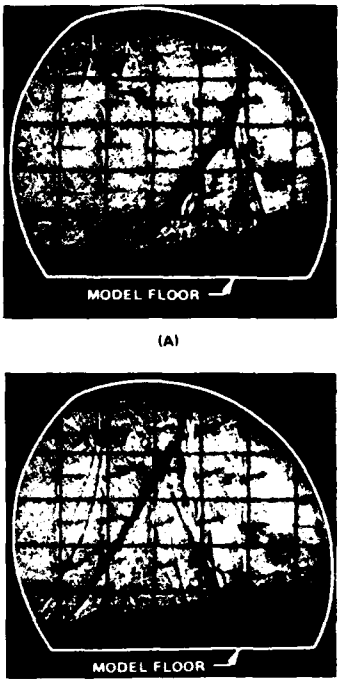

Fig. 13 Observed shock structures, 9.4% linearly tapered porosity.

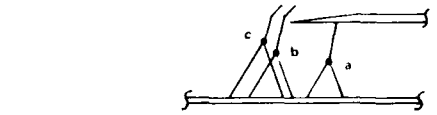

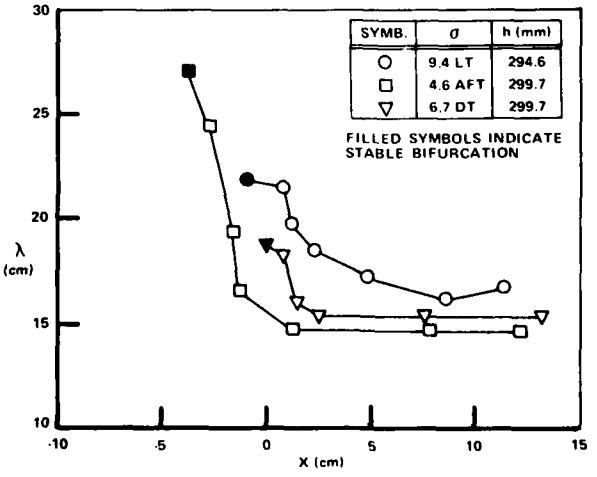

Fig. 14 Location of bifurcation point, M = 1.43, Re_L = 36 x 10^6.

show the deflection of boundary layer tufts which were mounted on the flow channel windows as a part of a concurrent corner flow investigation. They will not be discussed further here. Fig. 14 shows the variation in bifurcation height with distance along the flow channel for the porosities tested at $Re_L = 36 \times 10^6$. As the normal shock passes ahead of the holder lip, located at x = 4.4 cm, the forward movement of the bifurcation point is strongly reduced and its height increases rapidly, Fig. 13B (and position "c" in the sketch of Fig. 14). For the porosities that result in a stationary shock pattern, the height reaches a stationary value at that position which is indicated by the solid points in Fig. 14. It lasts until the end of the steady state test flow. The time period over which the shock was stable at the test position is indicated by the plot of λ height vs time shown in Fig. 15. Again the filled symbols indicate the stable shock position. In the three sets of data shown for porous shock holders the shock was stable for test times ranging from 15 to 25 msec. In the test with a solid top wall, the shock did not stabilize at all.

SYMB.	σ	h (mm)
▽	0	304.8
○	9.4 LT	294.6
□	4.6 AFT	299.7
△	6.7 DT	299.7

FILLED SYMBOLS INDICATE STABLE BIFURCATION

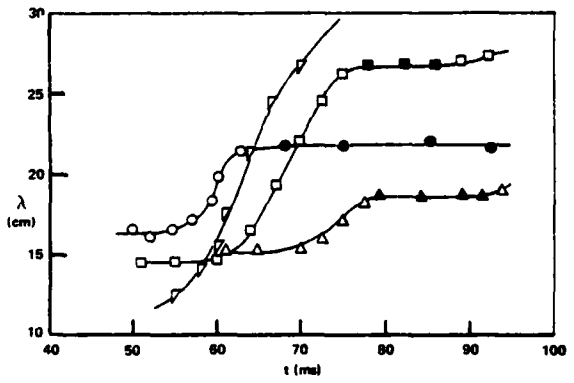

Fig. 15 Histories of bifurcation height, $Re_L = 36 \times 10^6$.

A possible factor in determining the height of a bifurcated shock structure is the degree of constraint applied to the streamline deflections behind the shock. During the period in which the shock remained within the shock holder flow channel, the bifurcation height remained nearly constant. In the 9.4% LT case, in which the local porosity increased to 12.5% as the shock moved forward, the increase in streamline deflection behind the shock produced a moderate continuing increase in the λ height. As the shock moved farther forward beyond the lip, the local effective porosity approached 100%, the streamline deflection increased, and the λ height increased sharply to an equilibrium value compatible with the spillage at the lip. For the other two porosities shown in Fig. 14 the porosity in the region $3 < x < 15$ cm was zero or nearly zero and the λ height was smaller than that in the 9.4% LT case. Furthermore, because the porosity was not varying, the λ height remained approximately constant until the shock moved forward of the shock holder lip. At that point the increasing streamline deflection due to spillage over the shock holder lip again caused a large increase in bifurcation height.

The data measured while the shock is moving through the shock holder flow channel strictly do not represent a steady flow case (as do the test points with the shock located at its stable position ahead of the shock holder lip). However the speed of the moving shock is small compared with the flow speed (≃5%), and the indicated trends are believed to be correct. In fact earlier comparisons between pressure data measured with slowly moving shocks and with stationary shocks show no significant difference.

Results of the test performed at $Re_L = 9 \times 10^6$ follow the same pattern. Both a constant height bifurcation slowly moving in the model and a constant height bifurcation stationary in front of the holder lip were observed. Fig. 16 shows their values and locations. Comparing the values inside the holder, it is found that they have increased at equal porosity as the Re_L has decreased. A similar trend was documented previously[3] for the area relief shock holder. The λ increase due to the Re_L decrease is about 30% for the porosity distributions 9.4 LT and 6.7 DT but only about 10% for the porosity 4.6 AFT. Not enough information is available at this stage to interpret this result.

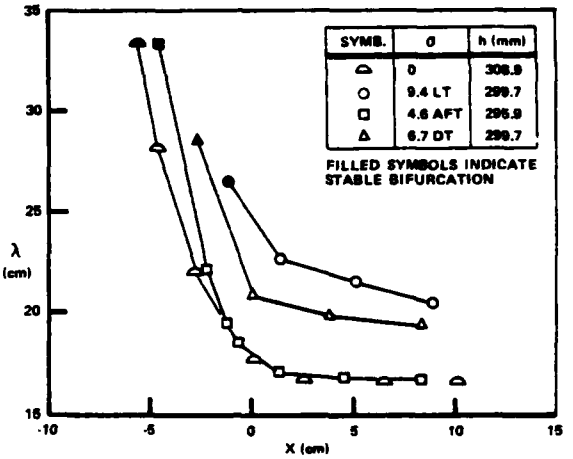

Fig. 16 Location of bifurcation point, M = 1.43, $Re_L = 9 \times 10^6$.

Wall pressures - During the investigation of the subsonic boundary effect, surface pressures were measured over the entire length of the model during each test. Pressure taps in the floor plate at fixed locations, more closely spaced at the lip, were used to this end. Additional measurements to fill in the basic coarse distribution were obtained when necessary by using the movable instrumented plate. Reading of pressure histories from each gauge at a fixed time produces a chronological description of the pressure rise in the model as the shock moves forward. Close to the lip the shock is in the field of view and direct correlation of wall pressure and bifurcation extent is possible.

The two constant height bifurcation phases, described previously in relation to the shock configuration, are found to have a precise correspondence in terms of surface pressures. When the bifurcation occurs inside the model, wall pressures are found to be very nearly self similar in distance. Thus the pressure level reached at any one fixed distance from the first rise is the same. As a result of the shock structure movement, however, the pressure at any fixed distance in the model frame of reference is continuously increasing. In particular this is true at the outlet of the model, where a maximum in wall pressure is reached only when the shock structure is expelled from the lip. The effect of porosity during this phase has yet to be fully analyzed. It is apparent however that a relationship exists between the observed bifurcation height and the slope of the sharp pressure rise. This follows the trend observed previously in connection with Reynolds number increases: smaller bifurcation heights correspond to sharper pressure rises.

When the bifurcation occurs in front of the model, no further changes take place in the wall pressure inside the holder. The forward movement of the shock structure to its stable position is associated in this phase with a reduction of the kink pressure level, with the non-linear pressure rise following the kink describing an envelope line that matches the extrapolation of the pressure distribution inside the holder. Most remarkable is the insensitivity of the wall pressures to the porosity distribution for all the interactions taking place in front of the lip. Fig. 17 shows the wall pressures recorded at a

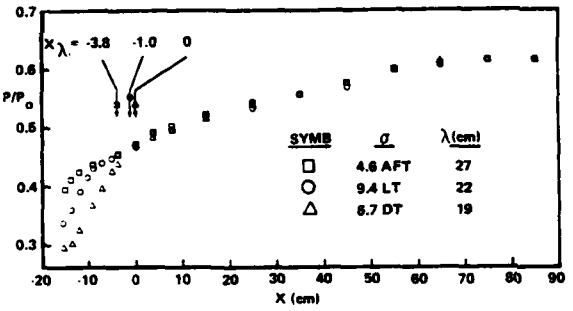

Fig. 17 Effect of subsonic boundary variations on wall pressure, $Re_L = 36 \times 10^6$.

Re_L of 36 x 10^6 and a fixed time of 82 msec when each porosity/flap condition shown has reached its stable shock configuration. There is no detectable effect of the porosity on the pressure distribution region located inside the holder. Outside of it the extent of the sharp pressure rise is reduced in proportion to the inverse of the bifurcation height. As a result the kink pressure value is reduced from $p/p_o = 0.45$ to 0.41 for σ = 6.7 DT to 4.6 AFT, respectively. The locations of the observed bifurcation point are also recorded in Fig. 17. Their position relative to the beginning of the sharp pressure rise corresponds to a description of the shock structures as having constant inclination of the forward shock leg and the measured bifurcation heights.

Figure 18 presents wall pressures recorded at $Re_L = 9 \times 10^6$ with shock structures in the stable

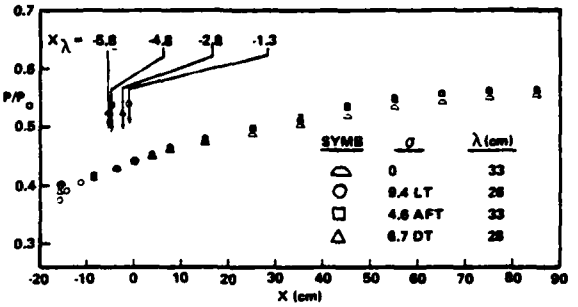

Fig. 18 Effect of subsonic boundary variations on wall pressure, $Re_L = 9 \times 10^6$.

positions of Fig. 16. The observations made at the higher Re_L regarding the chronology of pressure development in the model, effect of position relative to the lip and effect of porosity remain valid. However, at this Reynolds number the sharp pressure rise regions fall beyond the limits of the deployed instrumentation. The wall pressure distribution inside the holder is somewhat lower for the zero porosity case than for the other porosities. Here there is no suction whatsoever applied to the boundary layer growing at the top surface of the holder and a larger viscous blockage effect is to be expected. Disregarding this difference, direct comparison of Figs. 18 and 17 shows a major effect of Re_L on the wall pressure in the interaction. The rate of pressure recovery is lower everywhere at $Re_L = 9 \times 10^6$ resulting in a level of 77.8% of the normal shock value at 35 cm behind the lip. This value compares with a corresponding 83.8% in the $Re_L = 36 \times 10^6$ results.

Velocity profiles and streamline deflections - Throughout the subsonic boundary investigation tests, velocity profiles were also measured at a fixed location situated toward the rear of the model at X = 68 cm. Rakes of various heights were used to this end. The tallest rake spans the entire model height with 10 static and 10 pitot probes. For all the interactions generated with the porous shock holder the velocity profiles indicate a separated flow region near the model floor. Spot checks with the skin friction transducers at various downstream locations in the model concur to indicate that no reattachment takes place. The analysis of the velocity profiles measured is not complete. It is expected that their description of the transverse extent of the separation bubble will provide useful elements in the interpretation of the link between mass spillage at the lip and flow deflection controlling the interaction.

Streamline deflections 3.8 cm below the porous holder surface were measured directly with the flow angle probe for the 9.4 LT porosity distribution. The deflection measured was pitch in the vertical plane of symmetry of the model. In general, the histories show a stable upward flow first perturbed by a large upward increment, as the normal shock sweeps by, and then subsiding to a stable value larger than the undisturbed one. Streamline angles measured at three locations in the model are shown in Fig. 19. The open and filled symbols connected by a straight line represent flow deflections in the supersonic stream. They were

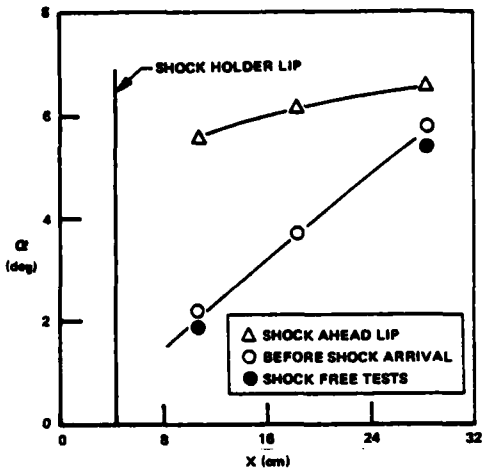

Fig. 19 Streamlines angle at 9.4 LT shock holder, $Re_L = 36 \times 10^6$.

measured both with a shock-free test flow (filled symbols) and using readings before the arrival of the shock. The open triangles represent the flow deflections measured with the shock in the stationary position in front of the holder lip. The transient values associated with the passage of the shock at the probe were found to correspond well with the deflections estimated on the basis of local shock inclination as indicated by the schlieren record.

Comparison with Previous Experiments

The results of the present investigation reveal that transonic shock-boundary layer interactions are significantly affected by the ratio of wall-to-total temperature and, for the configuration tested, by the geometry of the subsonic flow boundary downstream of the interaction as well as by the Reynolds number and Mach number investigated previously.

Vidal, Wittliff, Catlin and Sheen[3], Kooi[16], and Mateer, Brosh and Viegas[17] have shown the dependence of the surface pressure distribution on the Reynolds number ahead of the shock wave. In particular, Kooi compared his data obtained at $Re_L = 20 \times 10^6$ with Calspan data[3] obtained at 9×10^6 and 36×10^6 and observed that the initial pressure gradient increases with increasing Reynolds number. The data of Mateer confirms this dependence. Later, Kooi[18] showed that the pressure distribution, after the initial rapid rise, is dependent on the Mach number ahead of the shock wave. The present data show that the surface pressure distribution is independent of T_W/T_O when the streamwise distance is normalized by the undisturbed boundary layer thickness. The subsonic boundary condition investigation shows that the surface pressure distribution correlates directly with the height of the bifurcated shock structure. Variations in the constraints imposed on streamline deflections at the subsonic boundary result in changes in the height of the shock bifurcation. Taller bifurcations are found to correspond to smaller kink pressure values and to smaller slopes of the initial sharp pressure rise. The correlation between these changes in surface pressure and the height of bifurcation appears to hold in general. As pointed out, it is valid for increases in Re_L. This correlation also applies to the decrements in pressure which Kooi found occur with increases in M, which are associated with increases in λ. Kooi[16,18] has shown that the pressure rise at the foot of the shock can be computed using a "free interaction" formula up to the point of impingement of the rear shock on the viscous layer. The formula used links $d\delta^*/dx$ to M_δ (x) via a Prandtl-Meyer compression model. The present results do not contradict such calculation scheme. However they may restrict its applicability to a smaller distance at the shock foot.

The relationship measured in Calspan studies at $M \approx 1.43$ between the vertical and streamwise scales of the interaction characterized by λ and l_s, normalized by δ_u, is shown in Fig. 20. All of the data points in Fig. 20 were measured with the area relief shock holder. With the perforated shock holder installed the bifurcation height was found, as in the area relief case, to increase with decreasing Re_L (T_W/T_O = constant). With the shock structure in the same position within the 9.4 LT shock holder, the measured λ/δ_u values were 6.5 and 7.5 at $Re_L = 36 \times 10^6$ and 9×10^6 respectively. The separated region extended downstream beyond the available instrumentation and l_s/δ_u is known only to be greater than 20 for all of the data with the perforated shock holder.

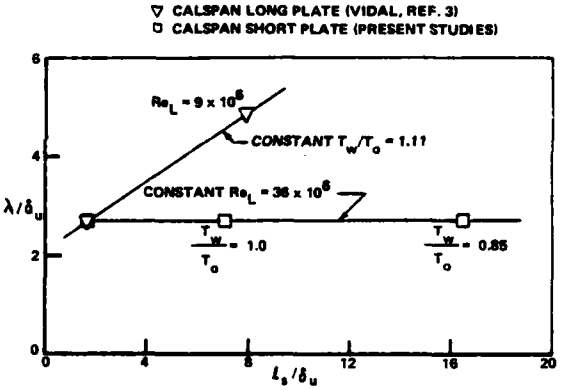

Fig. 20 Re_L and T_W/T_O effects on interaction lengths, M ~1.43.

Kooi[18] has compared the normalized separation length data of Seddon[9], Vidal, Wittliff, Catlin and Sheen[3,19], East[20], Sawyer[21] and Mateer, Brosh, and Viegas[17]. The Calspan data used in that comparison were taken at $T_W/T_O = 1.11$ and 1.0 (Refs. 3, 19), and Kooi did not note the dependence of normalized separation length on the temperature ratio. Kooi's comparison suggests that both the Mach number and Reynolds number have a strong influence on the extent of separation. The normalized separation length increases with increasing Mach number and decreases with increasing Reynolds number.

A comparison of normalized separation length as a function of Reynolds number Re_{δ_u}, similar to that made by Kooi, is shown in Fig. 21. Data obtained by Seddon[9], Kooi[16,18], East[20] and Sawyer, East and Nash[21] are compared with previous Calspan data and with present results. For each data point, the Mach number ahead of the shock and

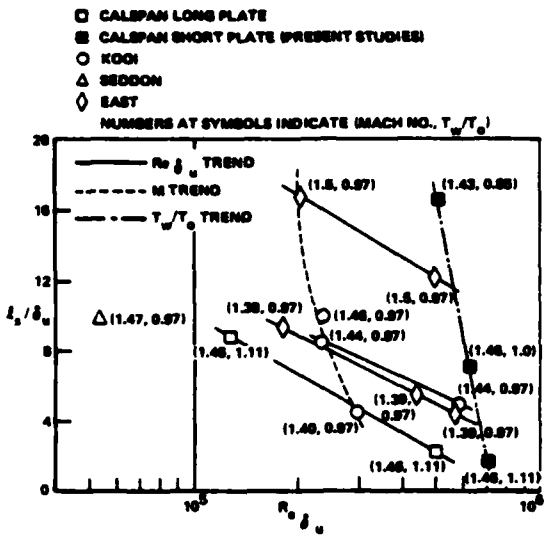

Fig. 21 Variation of l_s/δ_u with Re_{δ_u}, M, and T_w/T_o.

the temperature ratio T_w/T_o are noted in parentheses. As indicated above, Kooi's data at $Re\delta_u$ = 2.3 to 3.0 x 10^5 show the effect of Mach number on separation in that the separation length increases with Mach number, while the previous Calspan data at M = 1.46 and T_w/T_o = 1.11 and Kooi's data at M = 1.44 and T_w/T_o = 0.97 show that separation length decreases with increasing Reynolds number. In Fig. 21, the present data at Reynolds numbers based on δ_u from 5 x 10^5 and 7 x 10^5 illustrate the trend of increasing separation length with decreasing temperature ratio.

The results of the subsonic boundary investigation correspond to $Re\delta_u$ values of 5 x 10^5 and 1.3 x 10^5, at which separation lengths in excess of 20 occur. On the basis of all these data, it appears that separation length is much more sensitive to Mach number and temperature ratio than to Reynolds number.

Conclusions

Interactions of a normal shock with the turbulent boundary layer at M = 1.43, Re_L = 9 x 10^6 and 36 x 10^6 and T_w/T_o = 0.85, 1.0, and 1.11 have been investigated experimentally. In addition the effect of changing the subsonic boundary condition downstream of the interaction has been explored by using various amounts of porosity in the shock generator sustaining the shocked flow. The preliminary analysis of the data presently available has led to the following conclusions.

(A) With regard to the characteristic length scales of the interaction:

1. The normalized height of the bifurcated shock sturcture, λ/δ_u, does not depend on the wall-to-total temperature ratio in the range of values investigated. It decreases with increasing Reynolds number at fixed boundary condition, and it depends remarkably on constraints imposed on the deflection of the flow downstream of the interaction.

2. The normalized length l_s/δ_u of the separated flow region is found to decrease as the wall-to-total temperature ratio is increased. Reduction in the extent of separation behind the shock was obtained in past experiments by decreasing Mach number or by increasing the Reynolds number of the incoming flow. The length of separated flow region responds dramatically to the moderate but sustained flow deflections imposed by the perforated shock holders that were tested. No reattachment occurred in the present exploratory tests over a distance of over 20 undisturbed boundary layer thicknesses downstream of the interaction. Aggregate results from four applicable investigations of the variations of l_s/δ_u are still insufficient for an empirical formulation of the functional dependence of separation length on $Re\delta_u$, M and T_w/T_o. However, the stated trends are well defined. Furthermore, it is found that l_s/δ_u is much more sensitive to variations in Mach number and wall-to-total temperature ratio than Reynolds number.

(B) With regard to surface pressure distributions:

1. The surface pressure distribution has been found to be independent of wall-to-total temperature ratio when heat transfer effects on the incoming boundary layer are accounted for in the definition of the interaction boundary conditions (i.e. when streamwise distance is normalized by the undisturbed boundary layer thickness δ_u).

2. In general, the surface pressure distribution is found to correlate directly with the height λ of the bifurcated shock structure. Steep linear pressure rises to higher kink pressure levels are associated with small λ and vice versa. The effects of M, Re_L and the subsonic boundary condition on this height are thus reflected in the surface pressure distribution.

(C) With regard to surface skin friction:

1. Surface skin friction measurements using flush-mounted transducers have been used to determine the onset of boundary layer separation and reattachment. The onset of separation, relative to the location of the normal shock wave, was found to be independent of the temperature ratio, T_w/T_o. In contrast, reattachment moves farther downstream of the normal shock as T_w/T_o decreases.

References

1. Loving, D.L., "Wind-Tunnel-Flight Correlation of Shock-Induced Separated Flows," NASA-TN-D-3580, September 1966.

2. Pearcey, H.H., Osborne, J. and Haines, A.B., "The Interaction Between Local Effects at the Shock and Rear Separation - A Source of Significant Scale Effects in Wind-Tunnel Tests on Aerofoils and Wings," AGARD Conference Proceedings No. 35, Paper No. 11, 1968.

3. Vidal, R.J., Wittliff, C.E., Catlin, P.A. and Sheen, B.H., "Reynolds Number Effects on the Shock Wave-Turbulent Boundary-Layer Interaction at Transonic Speeds," AIAA Paper No. 73-661, AIAA 6th Fluid and Plasma Dynamic Conference, Palm Springs, CA, 16-18 July 1973.

4. Sheeran, W.J. and Hendershot, K.C., "A New Concept of a Variable-Mach Number Perforated Wall Nozzle for Providing a Supersonic External Stream in Rocket-Propulsion Testing," AIAA Paper 68-238, March 1968.

5. Davies, W.R. and Bernstein, L., "Heat Transfer and Transition to Turbulence in the Shock-Induced Boundary Layer on a Semi-Infinite Heat Plate," J. Fluid Mech., Vol. 36, Pt. 1, 1969, pp 87-112.

6. Bogdan, L., "Instrumentation Techniques for Short-Duration Test Facilities," Calspan Report No. WTH-030, March 1967.

7. Mac Arthur, R.C., "Contoured Skin Friction Transducers," Calspan Report No. AN-2403-Y-1, August 1967.

8. Waltz, A., Boundary Layers of Flow and Temperature, The M.I.T. Press, Cambridge, Massachusetts, 1969.

9. Seddon, J., "The Flow Produced by Interaction of a Turbulent Boundary Layer with a Normal Shock Wave of Strength Sufficient to Cause Separation," ARC R&M No. 3502, March 1960.

10. Adcock, J.B., Peterson, J.B., and McRee, D.I., "Experimental Investigation of a Turbulent Boundary Layer at Mach 6, High Reynolds Number and Zero Heat Transfer," NASA TN D-2907, July 1965.

11. Winter, K.G., and Gaudet, L., "Turbulent Boundary-Layer Studies at High Reynolds Numbers at Mach Numbers Between 0.2 and 2.8," R.A.E. RM No. 3712, December 1970.

12. Mabey, D.G., and Sawyer, W.G., "Experimental Studies of the Boundary Layer on a Flat Plate at Mach Numbers from 2.5 to 4.5," R.A.E. RM No. 3784, September 1974.

13. McNally, W.D., "Fortran Program for Calculating Compressible Laminar and Turbulent Boundary Layers in Arbitrary Pressure Gradients," NASA TN D-5681, May 1970.

14. Padova, C., and Wittliff, C.E., "The Effects of Wall-to-Total Temperature Ratio on Shock Wave-Turbulent Boundary Layer Interactions at Transonic Speeds," Calspan Report No. WF-6091-A-1, October 1979.

15. Little, B.H., "Effects of Initial Turbulent Boundary Layer on Shock-Induced Separation in Transonic Flow," von Karman Institute for Fl. Dyn., Tech. Note 39, October 1967.

16. Kooi, J.W., "Experiment on Transonic Shock-Wave Boundary Layer Interaction," AGARD CP-168 (also, NLR MP 75002 U), 1975.

17. Mateer, G.G., Brosh, A. and Viegas, J.R., "A Normal Shock-Wave Turbulent Boundary-Layer Interaction at Transonic Speeds," AIAA Paper No. 76-161 presented at the AIAA 14th Aerospace Sciences Meeting held in Washington, D.C., January 26-28, 1976.

18. Kooi, J.W., "Influence of Free-Stream Mach Number on Transonic Shock-Wave Boundary-Layer Interaction," NLR MP 78013 U, 23 May 1978.

19. Vidal, R.J. and Catlin, P.A., "Investigations of Shock Wave-Turbulent Boundary Layer Interactions at Transonic Speeds," Calspan Report No. WF-5746-A-1, April 1977.

20. East, L.F., "The Application of a Laser Anemometer to the Investigation of Shock-Wave Boundary-Layer Interactions," AGARD CP-193, May 1976.

21. Sawyer, W.G., East, L.F. and Nash, C.R., "A Preliminary Study of Normal Shock-Wave Turbulent Boundary-Layer Interactions," RAE Tech. Memo 1714, June 1977.